Supporting Information

Anti-fouling Nanoplasmonic SERS Substrate for Trapping and Releasing Cationic Fluorescent Tag from Human Blood Solution

Kundan Sivashnamugan[1], Po-Chun Liu[1], Kai-Wei Tsai[1], Ying-Nien Chou[1], Chen-Hsueh Lin[1], Yung Chang[2], Ten-Chin Wen[1,]*

[1] Department of Chemical Engineering, National Cheng Kung University, Tainan 70101, Taiwan

[2] R&D Center for Membrane Technology and Department of Chemical Engineering, Chung Yuan Christian University, Chung-Li, Taoyuan 320, Taiwan

[*]Corresponding author.

E-mail: tcwen@mail.ncku.edu.tw

Supporting information contents:

1. Experimental section

1.1. Materials

Silver trifluoroacetate (CF_3COOAg), poly(vinylpyrrolidone) (PVP; $M_{n=55,000}$), sodium hydrosulfide (NaSH), ethylene glycol (EG), glycidyl methacrylate (GMA), azobisisobutyronitrile (AIBN), and methanol were purchased from Sigma-Aldrich. Human plasma fibrinogen (fraction I), primary monoclonal antibody, and secondary monoclonal antibody were purchased from Sigma Chemical Co, USA. [2-(methacryloy loxy)ethyl]-dimethyl-(3-sulfopropyl)-ammonium hydroxide (sulfobetaine methacrylate, SBMA) was purchased from Monomer-Polymer & Dajac Laboratories, Inc., USA. Ultra-pure water (≈10 MΩ·cm) was used as a solvent in the experiments.

1.2. Synthesis of Ag nanocubes

The synthesis of size-controlled Ag NCs was conducted via the modified polyol process[1]. EG and NaSH with analytical-grade purity were used as the starting materials without further purification. Typically, 5 mL of EG was added into a 100-mL round-bottom flask and heated under magnetic stirring in a 160 °C oil bath for 1 h. Next, 0.06 mL of 3 mM NaSH solution was rapidly injected into the heated EG with continuous heating for 10 min. To this mixture solution, 0.5 mL of HCl solution (3 mM) was added rapidly under vigorous stirring. After 2 min, 1.25 mL of PVP (20 mg/mL in EG) solution was injected into the heated reaction solution, followed by the addition of 0.4 mL of CF_3COOAg (282 mM in EG) solution. The solution mixture was heated and stirred until a color change became evident. Subsequently, the reaction was stopped by placing the reaction flask in an ice-water bath. The solution was removed and brought to room temperature, and then washed five times using water and acetone to remove impurities and used for further studies. Finally, the as-prepared Ag NCs were stored at under 4 °C for further use. The morphology

and optical properties of the as prepared Ag NCs were characterized using FESEM, HR-FETEM and UV-Vis spectrophotometry.

1.3. Synthesis of poly(GMA-*co*-SBMA) copolymers

The copolymer poly(GMA-*co*-SBMA) was synthesized according to the reported procedure as follows[2]. GMA and SBMA monomers at a molar ratio of 20:80 were dissolved in methanol and water to form a 1 M solution under continuous stirring. The obtained mixture solution was purged through N_2 gas for 15 min. To this mixture solution, the weight content of 1% eq. of AIBN was then added rapidly under vigorous stirring for another 15 min. Then the reaction mixture solution was stirred for 6 h at 60 °C. The resulting solution was cooled to 4 °C for longer than 3 h (**Scheme S1**). After polymerization, a white precipitate was found in the reacted solution; which was filtered and dried; then the resulting copolymer was purified by dissolving in water and precipitate in methanol for three times. The copolymer was dried in a freezer using a lyophilizer; the copolymer poly(GMA-*co*-SBMA) was obtained as white powder and was stored at 4 °C until use.

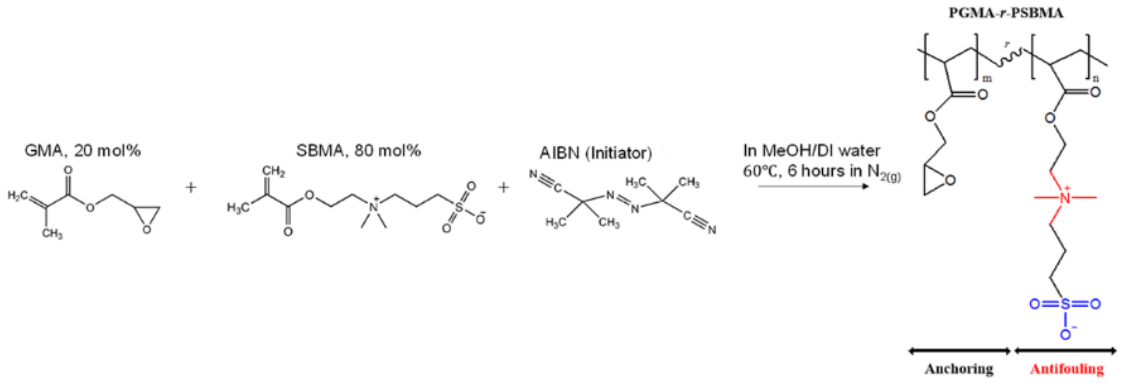

Scheme S1 Reaction scheme for poly(GMA-*co*-SBMA).

The molecular weight of poly(GMA-*co*-SBMA) was determined using aqueous gel-permeation chromatography (GPC; Viscotek GPCmax Module, USA). The GMA/SBMA molar ratio was calculated according to the relative ^{1}H NMR peak area of the epoxide side group of the GMA segments and the $(CH_3)^2N^+$ proton resonance of the SBMA segments. The details are discussed in

our previous paper[2]. Poly(SBMA) provides anti-fouling for a bio-target-attached surface due to its strong surface hydration barrier. Poly(GMA) facilitates grafting via reactive chemisorption (i.e., covalent bond formation), which increases the stability and coverage of zwitterionic copolymers on the biomaterial surface.

1.4. Platelet-rich plasma adhesion and adsorption

The poly(GMA-*co*-SBMA)-grafted MIM substrates were placed in individual wells of a 24-well tissue culture plate. To each well was added 1000 μL of PBS for 2 h at 37 °C. PRP was obtained from a healthy volunteer. The platelet concentration was determined using a microscope (NIKON TS 100F). The poly(GMA-*co*-SBMA)-grafted MIM substrate surfaces and 800 μL of PRP was added to each well, which was then incubated for 2 h at 37 °C. The prepared substrates were rinsed twice with 1000 μL of PBS and immersed into 2.5% glutaraldehyde of PBS for 48 h at 4 °C to fix the adhered platelets. The adhesion of PRP to substrates was observed using CLSM, with images taken at a 200× magnification from 6 sites on each sample.

The fouling level for PRP was evaluated using the ELISA. The detailed procedure is explained elsewhere[2-3]. The poly(GMA-*co*-SBMA)-grafted MIM substrates were placed in individual wells of a 24-well tissue culture plate. To each well was added 1000 μL of PBS for 1 h at 37 °C; each well was then soaked in PRP solution (500 μL). The prepared substrates were rinsed twice with 1000 μL of PBS and then incubated in bovine serum albumin for 2 h at 37 °C to block the areas unoccupied by protein. Furthermore, the poly(GMA-*co*-SBMA)-grafted MIM substrates were rinsed with PBS and changed to a new plate and incubated in PBS (1000 μL) solution with a primary monoclonal antibody that reacted with the fibrinogen for 2 h at 37 °C. The poly(GMA-*co*-SBMA)-grafted MIM substrates were subsequently incubated with the secondary monoclonal antibody, horseradish-peroxidase-conjugated immunoglobulins, for 1 h at 37 °C. After the removal

of the unbonded reagent from GS(0,1,5,10, 15)-MIM substrates and transfer to clean wells, 0.5 mg/mL of 3,3',5',5'-tetramethylbenzidine solution was added to the wells, which were incubated for 8 min. Then, 500 μL of mmol/mL H_2SO_4 solution was added to each well. The plate was finally read using a microplate reader at an absorbance of 450 nm. PRP adsorption on the poly(GMA-*co*-SBMA)-grafted MIM substrates was normalized with respect to that on the virgin substrate as a reference. These measurements were carried out six times for each substrate (n = 6).

2. Formation of poly(GMA-*co*-SBMA) grafted onto MIM substrate surface

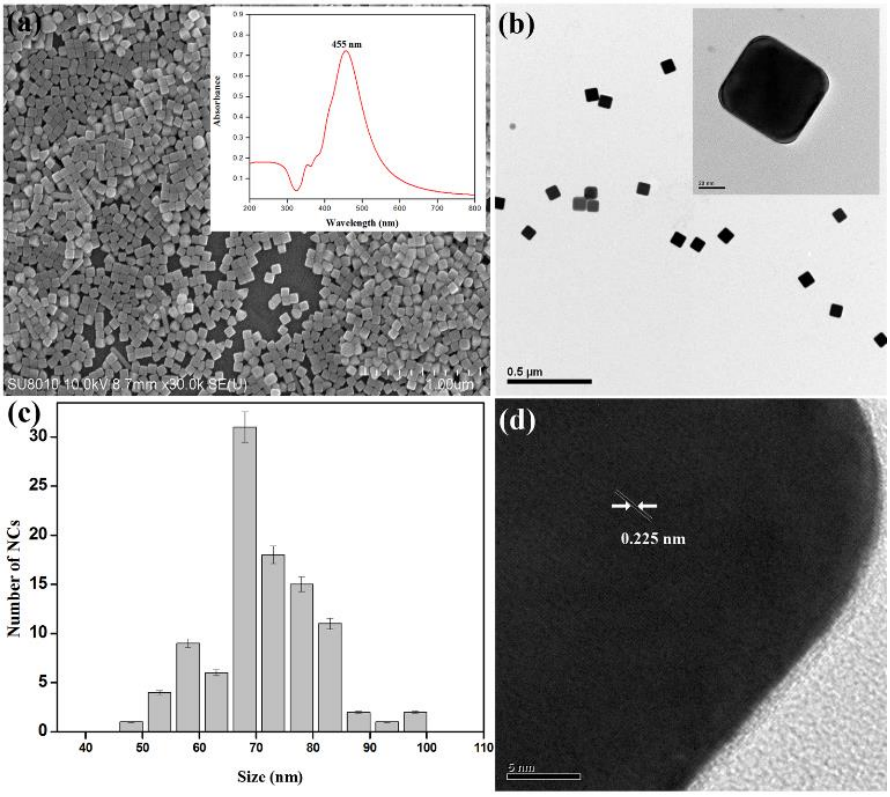

Figure S1 (a) FESEM image of as-synthesized Ag NCs. Inset figure shows UV absorbance spectrum of as-synthesized Ag NC solution. (b) HR-TEM image of as-prepared Ag NCs, (c) their overall size distribution histogram, and (d) lattice image.

Ag NCs were synthesized via the polyol method[1]. The as-synthesized Ag NCs exhibited plasmon resonance at 455 nm, suggesting that they were dispersed in the aqueous solution without aggregation. This observation confirms that the as-synthesized Ag NCs were mostly of nanometer size. The Ag NCs were uniformly shaped cubes with a mean edge length of 70 nm, as shown in **Figure S1**. Furthermore, a crystalline Ag lattice perfectly formed with a lattice spacing of 0.225 nm, which fits with the face-centered cubic plane[4].

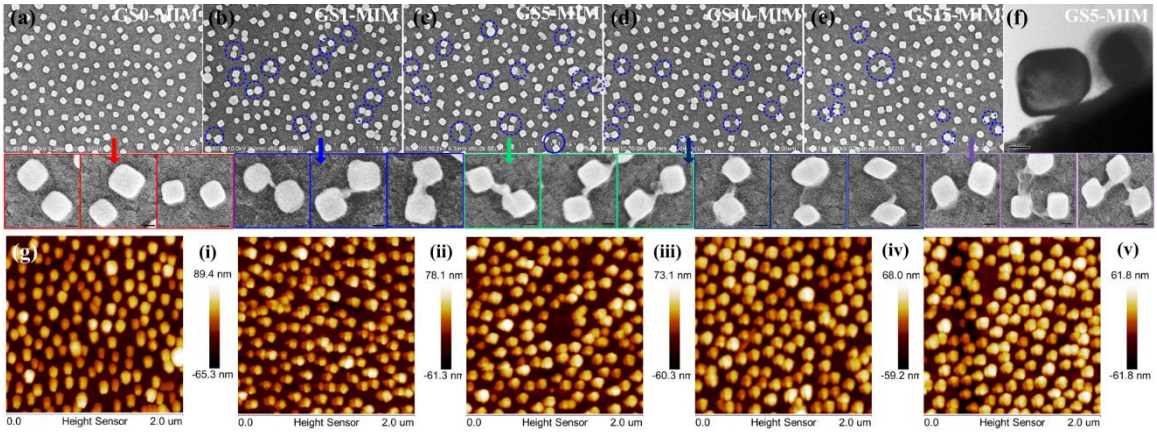

Figure S2 FESEM images of as-fabricated poly(GMA-*co*-SBMA) of various concentrations grafted onto MIM substrates (a) GS0-MIM, (b) GS1-MIM, (c) GS5-MIM, (d) GS10-MIM, and (e) GS15-MIM. Bottom row shows marked positions in FESEM images enlarged to confirm connection between two adjacent NCs via poly(GMA-*co*-SBMA) graft (scale bar: 100 nm). (f) HR-FETEM image of poly(GMA-*co*-SBMA) grafted between two adjacent NCs. (g) AFM topography of as-fabricated poly(GMA-*co*-SBMA) grafted samples.

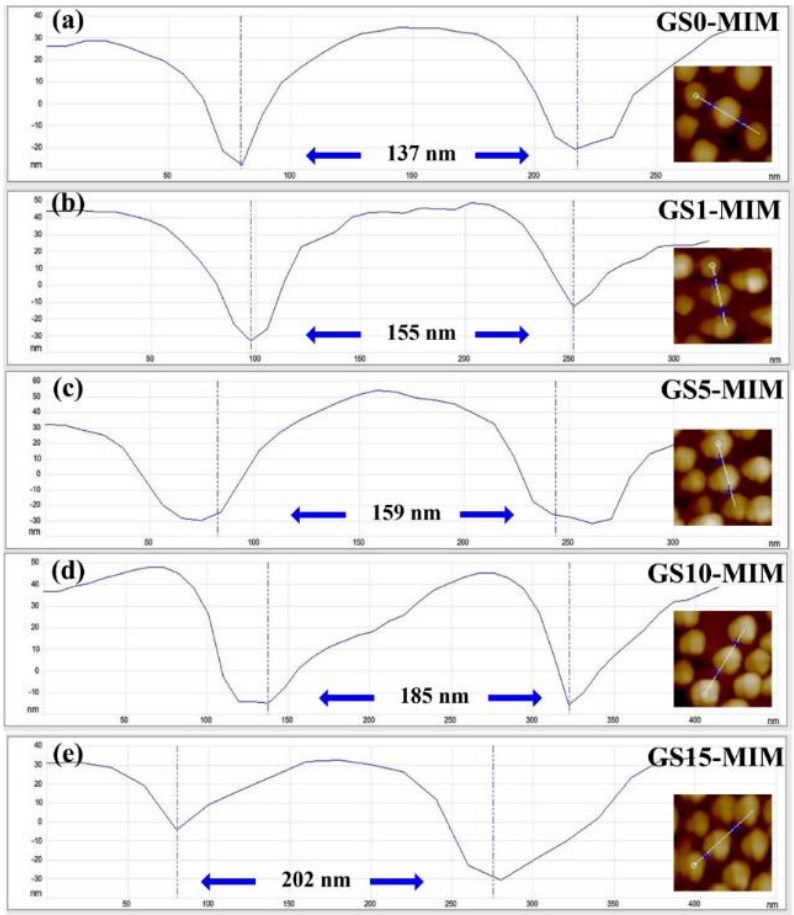

Figure S3 AFM line profiles of as-fabricated poly(GMA-*co*-SBMA) of various concentrations grafted onto MIM substrates (a) GS0-MIM, (b) GS1-MIM, (c) GS5-MIM, (d) GS10-MIM, and (e) GS15-MIM. Inset AFM topography images show measured area of line profile.

Table S1 Contact angle, roughness, intercube distance, and SPR shift of as-fabricated copolymer MIM substrates.

Sample	Contact angle (◦)		Roughness (nm)	Intercube distance (nm)	SPR shift (nm)
	Water	PBS			
GS0-MIM	45.46	36.64	24.6	58	584
GS1-MIM	14.82	10.92	21.3	24	599
GS5-MIM	14.16	11.56	22.1	49	616
GS10-MIM	20.56	14.78	22.8	56	582
GS15-MIM	21.70	18.74	21.0	73	582

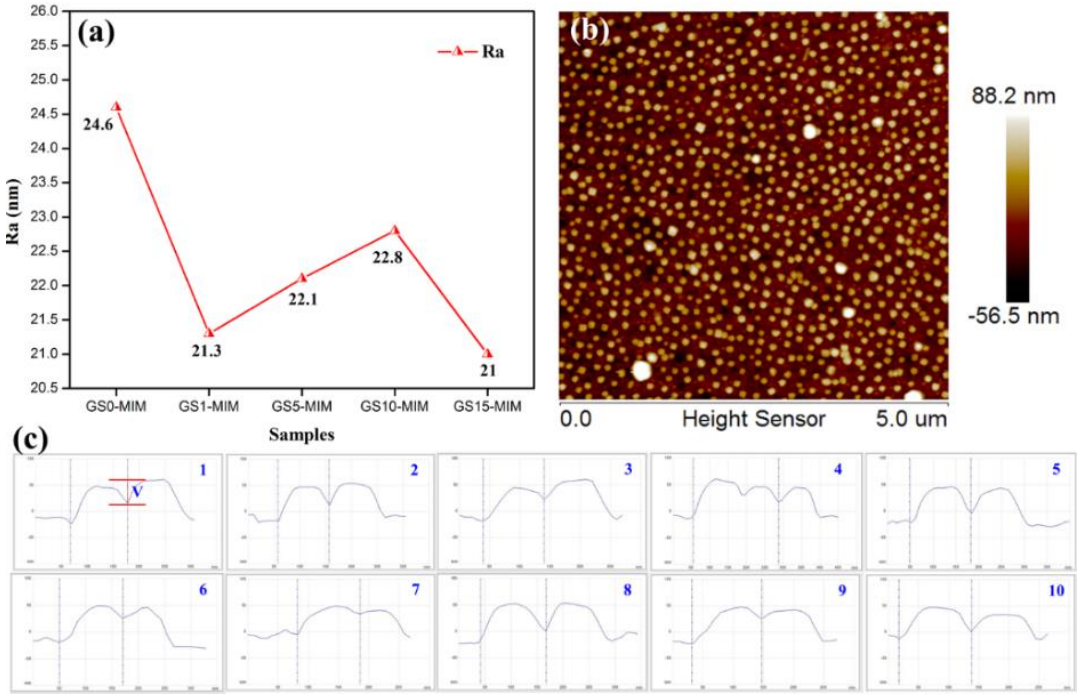

Figure S4 (a) Roughness of as-fabricated poly(GMA-*co*-SBMA) with various concentrations grafted onto MIM substrates (GS0-MIM , GS1-MIM, GS5-MIM, GS10-MIM, and GS15-MIM). The poly(GMA-*co*-SBMA)-grafted sample surface roughness was lower than that of the sample without a copolymer surface, which confirmed copolymer grafting, as shown in **Table S1**. AFM topography of (b) GS5-MIM and (c) corresponding AFM line profile at many positions. Marked area was significantly varied (denoted V) in poly(GMA-*co*-SBMA) grafted between two adjacent NCs.

3. Plasmonic enhancement from MIM substrate surface

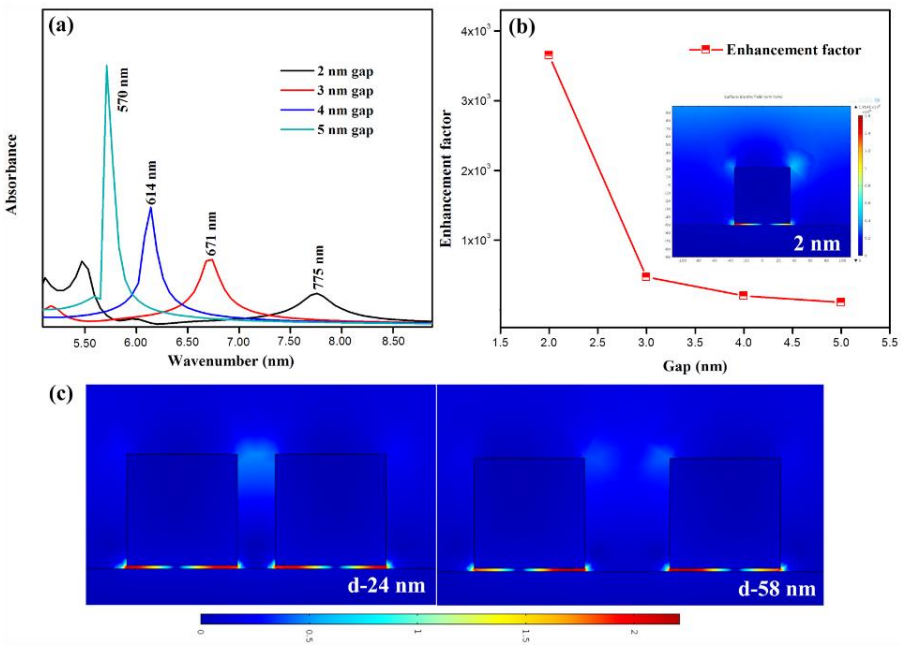

Figure S5 (a) Scattering spectra and (b) enhancement factor (inset shows local field distributions) for Ag NCs atop Ag film calculated using commercial software COMSOL. (c) Local EM field distributions for face-to-face adjacent NCs calculated using commercial software COMSOL.

COMSOL was used to calculate the surface plasmon resonance (SPR) shift and local field distributions on the MIM surface. Our previous simulation results showed that the strong plasmonic effect has confined in the gaps between the Ag NCs and Ag film[5-6]. In **Figure S5(a)**, Ag NCs with edge lengths of 70 nm were placed on Ag film with gaps of 2, 3, 4, and 5 nm, respectively. **Figure S5(a)** shows the calculated scattering spectrum of the MIM substrate with gaps of 2, 3, 4, and 5 nm, respectively. The strong SPR peaks at 775, 671, 614, and 570 nm for samples with different gaps show that plasmonic coupling of NCs was related to the dielectric constant of the surrounding environment[7]. The EF decreased with increasing gap width in the MIM geometry, which is consistent with the intensity in the simulated absorption spectra, as shown in **Figure S5(b)**. Therefore, the spacer plays a very important role in the MIM substrate. The strong

local field distributed at the corners of the NCs is shown in the inset of **Figure S5(b)**. In our experiments, a 2-nm gap width was chosen for the investigation of the shape effect of NCs for further studies.

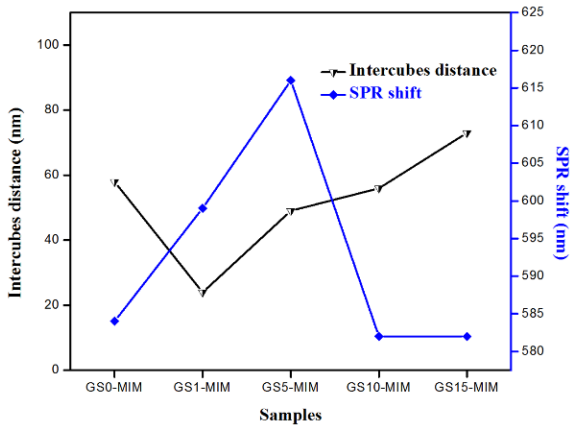

Figure S6 Relation between intercube distance and SPR shift of copolymer-grafted MIM substrates.

4. Anti-fouling studies of poly(GMA-*co*-SBMA)-grafted MIM substrate surface

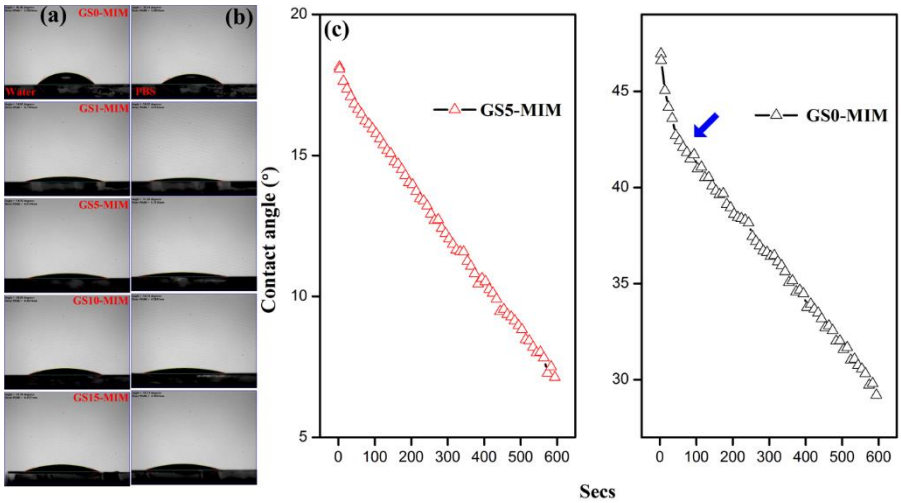

Figure S7 Contact angle images of (a) water and (b) PBS for all samples. (c) Water solution rapidly diffused on poly(GMA-*co*-SBMA)-grafted MIM substrate surface as compared with GS0-MIM

surface. Water solution on copolymer-grafted surface required shorter time to reach equilibrium compared to that obtained without a copolymer-grafted surface due to hydrophilic surface.

5. Distinguishing surface hydration in poly(GMA-*co*-SBMA)-grafted MIM substrate surface

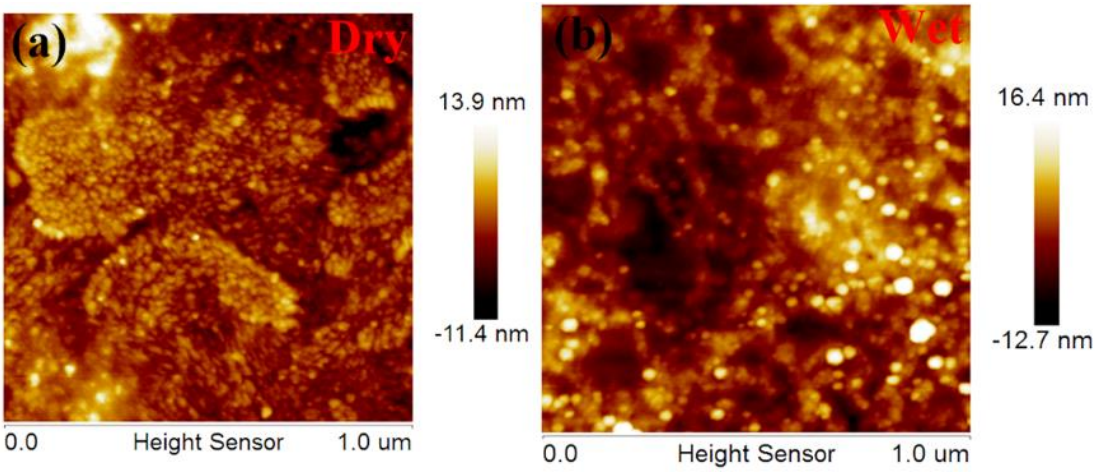

Figure S8 AFM topography images of (a) non-hydrated and (b) surface hydrated conditions of copolymer-grafted MIM substrate surface.

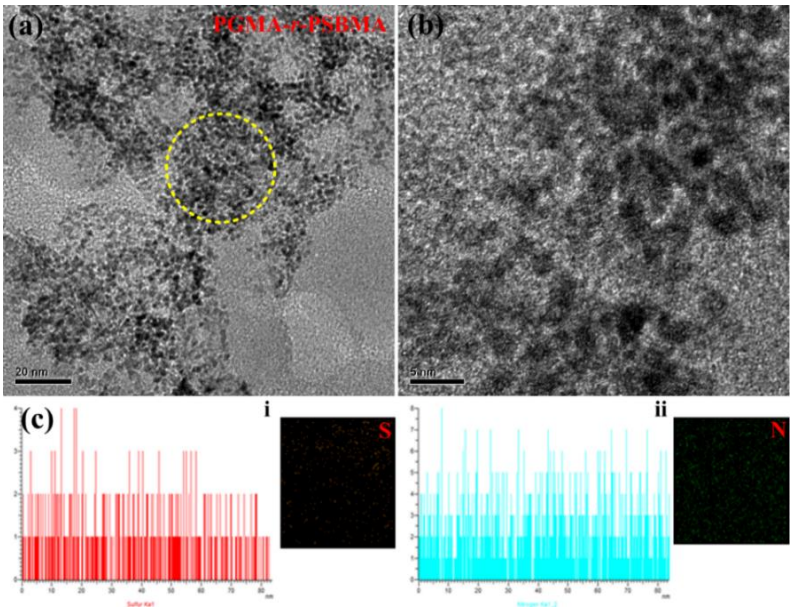

Figure S9 HR-FETEM images of (a, b) copolymer and (c) EDS mapping from marked area in (a). Different contrast regions indicate ionic crosslinks at surface, which were confirmed by EDS mapping.

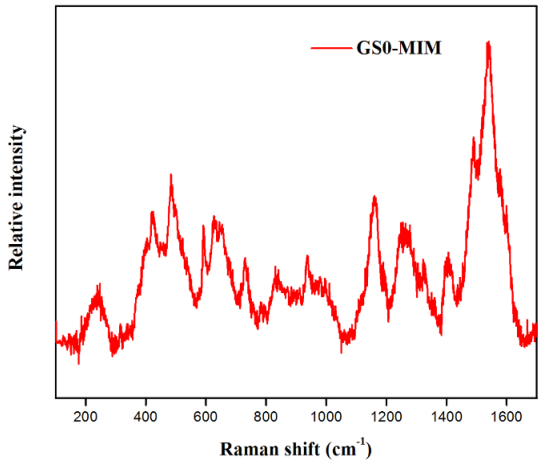

Figure S10 Ag NCs on Ag film substrate examined at Raman laser wavelength of 633 nm.

Table S2 Raman assignment of copolymer-grafted MIM substrate surface

Raman shift (cm^{-1})			Assignment
Non-hydrated	**Surface hydrated**	**Dehydrated**	
	1600-1800*		H-C=O, O-C=O stretching
1605 1563 1518	1576	1601	O-C=O stretching
	1400-1500*		CH_2 bending
1369 1336	1360 1337	1370 1314	O-C=O stretching
1281	1269	1289	S=O, $-SO_3$ stretching
1152	1174	1187 1154	-SO3 stretching
1074	1072	1100 1097	$-SO_3$ stretching
1034	1034	1028	C_4N^+ stretching

*For all conditions

Table S3 Raman assignment of MIM substrate surface

Raman shift (cm^{-1})	Assignment
1710, 1668, 1599	C=O stretching
1599	N-C=O stretching
1538	C-N
1489	C-N
1402	CH_2 bending
1325	CH_2 wagging
1264	CH_2 sissor, C-N stretch
1160	CH_2 twisting
937	CH_2 rocking
835	C-C ring
731	T-CS stretching
650	G-CS stretching
626	G-CS stretching
241	Ag-S stretching

6. Detection of MG in complex biosystem

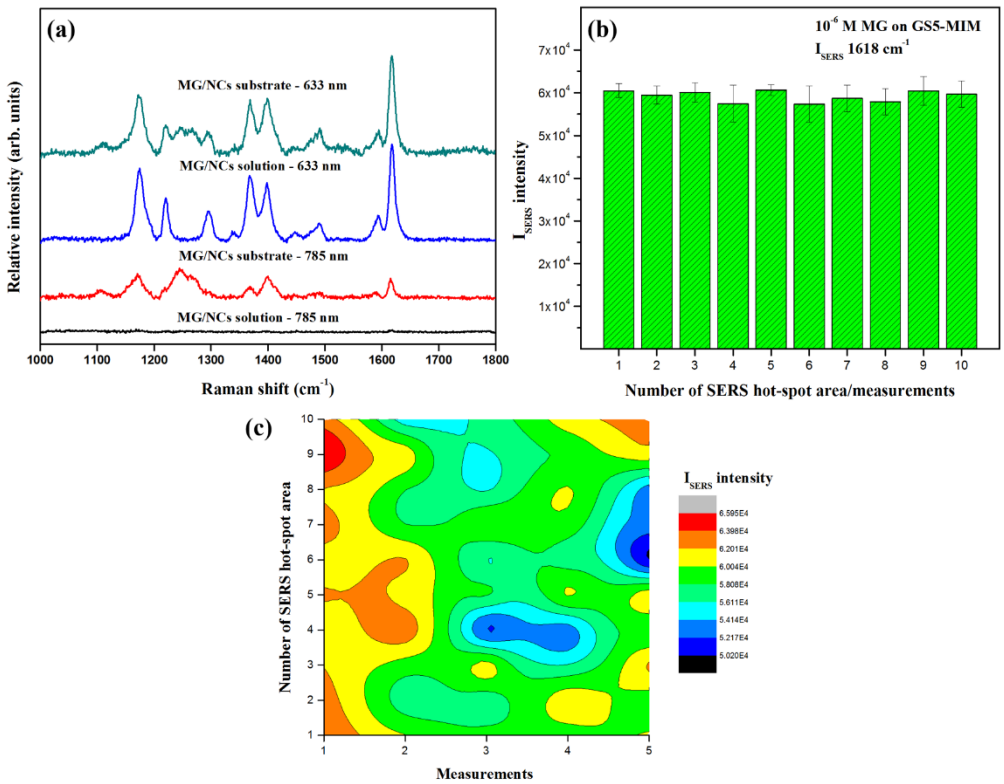

Figure S11 Raman-active peaks of 5×10^{-6} M MG in Ag NC solution and on Ag NCs on Ag film substrate examined at Raman laser wavelengths of 633 and 785 nm (a). Raman-active peaks of

5×10^{-6} M MG in PBS solution on GS5-MIM samples obtained at Raman laser wavelength of 633 nm. Relative Raman intensity versus 1 to 10 SERS hot-spot area (i.e., sampling positions) and each spot five continues Raman measurement from substrates examined by a Raman laser wavelength of 633 nm (b). Color distribution of Raman intensity (I_{SERS}- 1618 cm^{-1}) from 10 SERS hot-spot area (i.e., sampling positions) and each spot five continues Raman measurement under 633 nm Raman laser (c).

Figure S11 shows Raman spectra of MG with a concentration of 5×10^{-6} M MG in Ag NC solution and on Ag NCs on an Ag film sample determined at laser wavelengths of 633 and 785 nm. The most intense Raman shifts from the characteristic peaks of MG (I_{sers}) usually appeared at 1618 cm^{-1}, which are assigned to the ring C-C stretching modes. Ag NC solution and Ag NCs on Ag film samples exhibited higher I_{sers} values under a laser wavelength of 633 nm compared to those for a laser wavelength of 785 nm. The energy for a Raman laser wavelength of 633 nm matches the substrate plasmonic band, enhancing Raman scattering. To study the SERS hot-spot distribution on GS5-MIM substrate, Raman spectra of MG upon the GS5-MIM substrate exhibited greatly enhanced without significant difference in multiple SERS hot-spot area, as shown in **Figure S11 (b) and (c)**.

The SERS signal for the GS0-MIM (i.e., without copolymer) with PRP evaluated at Raman laser 633 nm, as shown in **Figure S12(a)**. The average SERS peaks of PRP appeared at 1028, 1158, 1174, 1201, 1451, and 1600 cm^{-1}. These SERS spectra from PRP components such as lipids, nucleic acids, and protein. PRP on poly(GMA-*co*-SBMA)-grafted MIM substrate was examined using a laser wavelength of 633 nm. We observed a very weak Raman signal from PRP on the substrate due to non-specific adsorption, as shown in **Figure S12(a)**. To verify other types of molecule SERS detection on poly(GMA-*co*-SBMA)-grafted MIM substrate, Raman spectra of

aminothiophenol (ATP) (10^{-5} to 10^{-9} M, PRP solution) on GS5-MIM substrate was examined at laser wavelength of 633 nm, as shown **Figure S12 (b)**. The strong SERS characteristic peaks of 4-ATP appeared at 1080 cm^{-1}, which was assigned to the C-S stretching of ATP. The results indicates that the ATP molecule can be chemically adsorbed on copolymer grafted surface due to chemisorption of the thiol group and enhance the SERS signal.

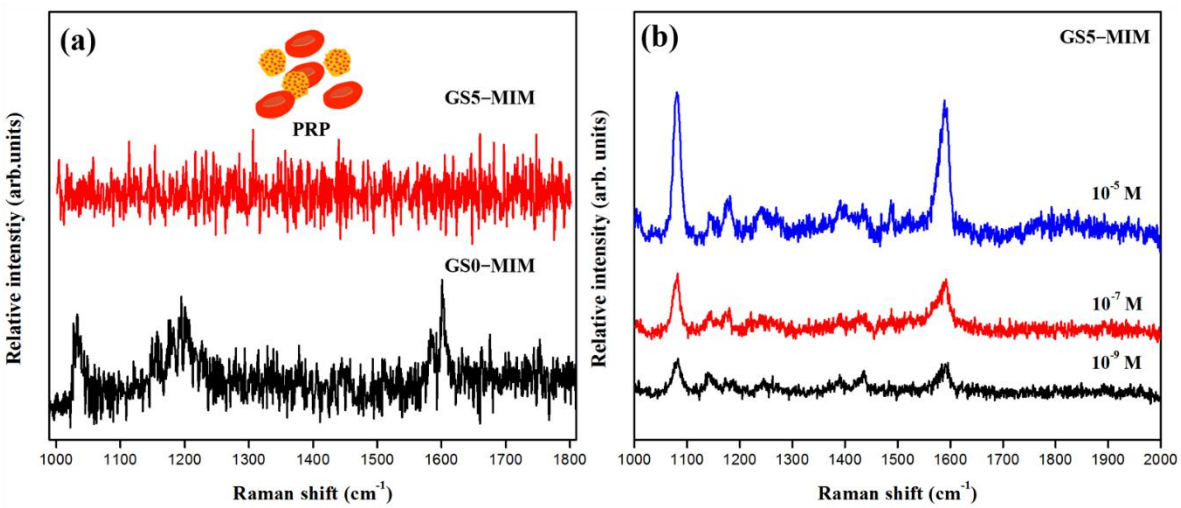

Figure S12 PRP solution on poly(GMA-*co*-SBMA)-grafted MIM substrates surface examined at Raman laser wavelength of 633 nm (a). Raman-active peaks of ATP (10^{-5} to 10^{-9} M) in PRP solution on GS5-MIM samples obtained at Raman laser wavelength of 633 nm.

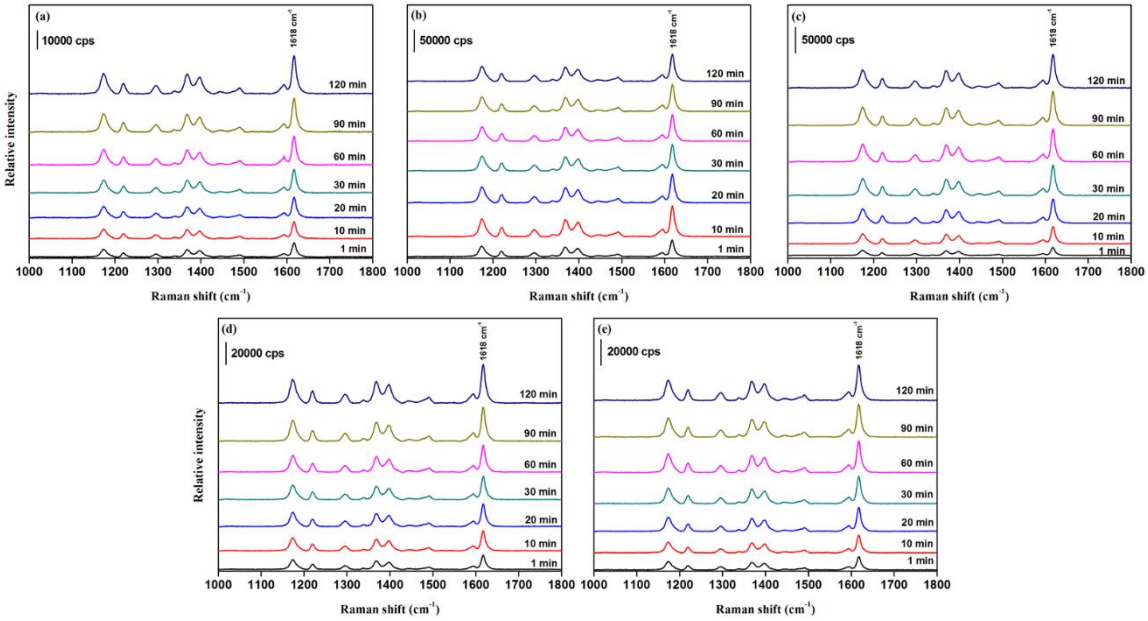

Figure S13 (a-e) Raman-active peaks of 5×10^{-6} M MG in PBS solution on poly(GMA-*co*-SBMA)-grafted MIM substrates examined at laser wavelength of 633 nm at various times.

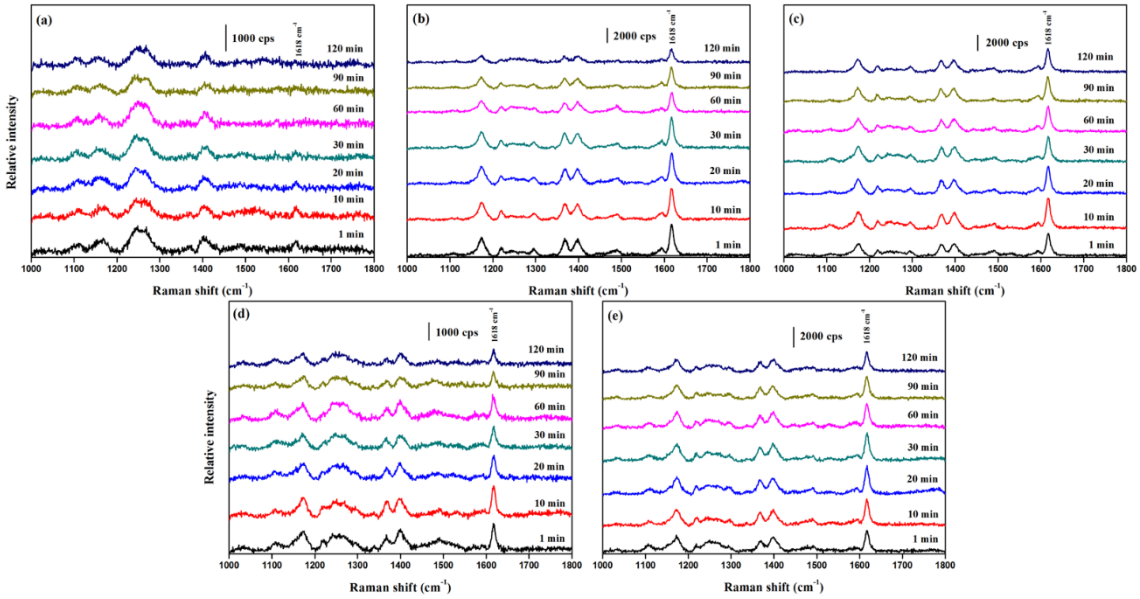

Figure S14 (a-e) Raman-active peaks of 5×10^{-6} M MG in PRP solution on poly(GMA-*co*-SBMA)-grafted MIM substrates examined at laser wavelength of 633 nm at various times.

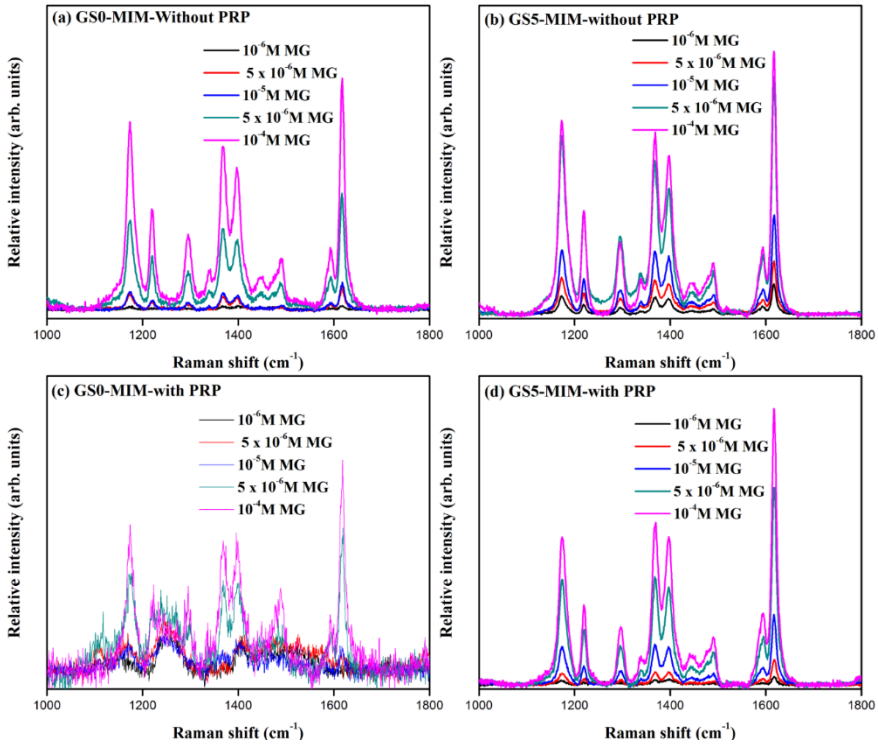

Figure S15 Raman-active peaks of MG at various concentrations in (a, b) PBS and (c, d) PRP solutions on GS0-MIM and GS5-MIM substrates examined at Raman laser wavelength of 633 nm.

MG at various concentrations in PBS and PRP solutions on GS0-MIM and GS5-MIM substrates was tested. **In Figure S15**, the most intense Raman shifts from the characteristic peak of MG in PBS or PRP solution on GS0-MIM and GS5-MIM samples appeared at 1618 cm^{-1}. The GS5-MIM sample SERS effect was enhanced compared to that of GS0-MIM, as shown in **Figure S16**. The copolymer grafted between two intra-NC surfaces can change the local field effect and enhance SERS signals.

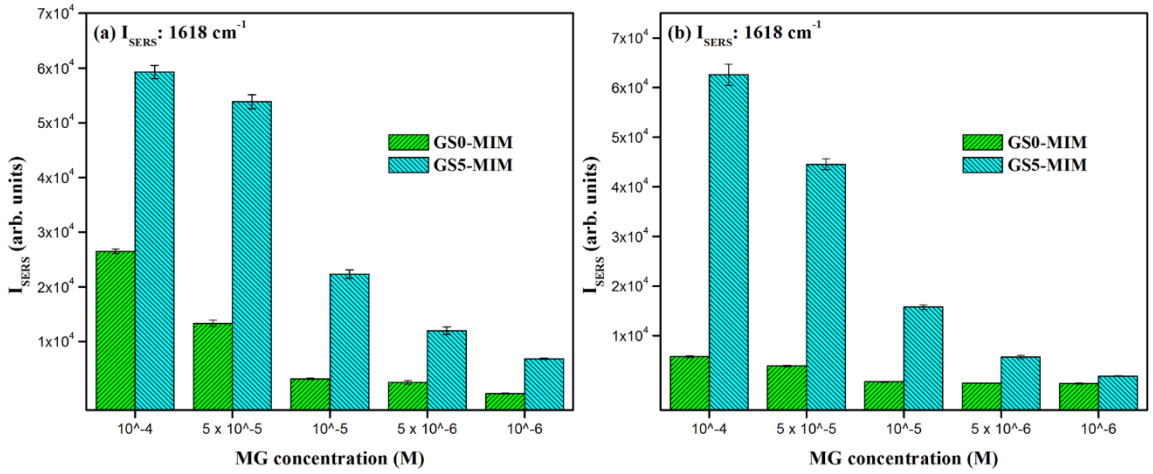

Figure S16 MG SERS peak at 1618 cm^{-1} used as index for relative Raman intensities for various samples and concentrations of MG in PBS (a) or PRP (b) solution.

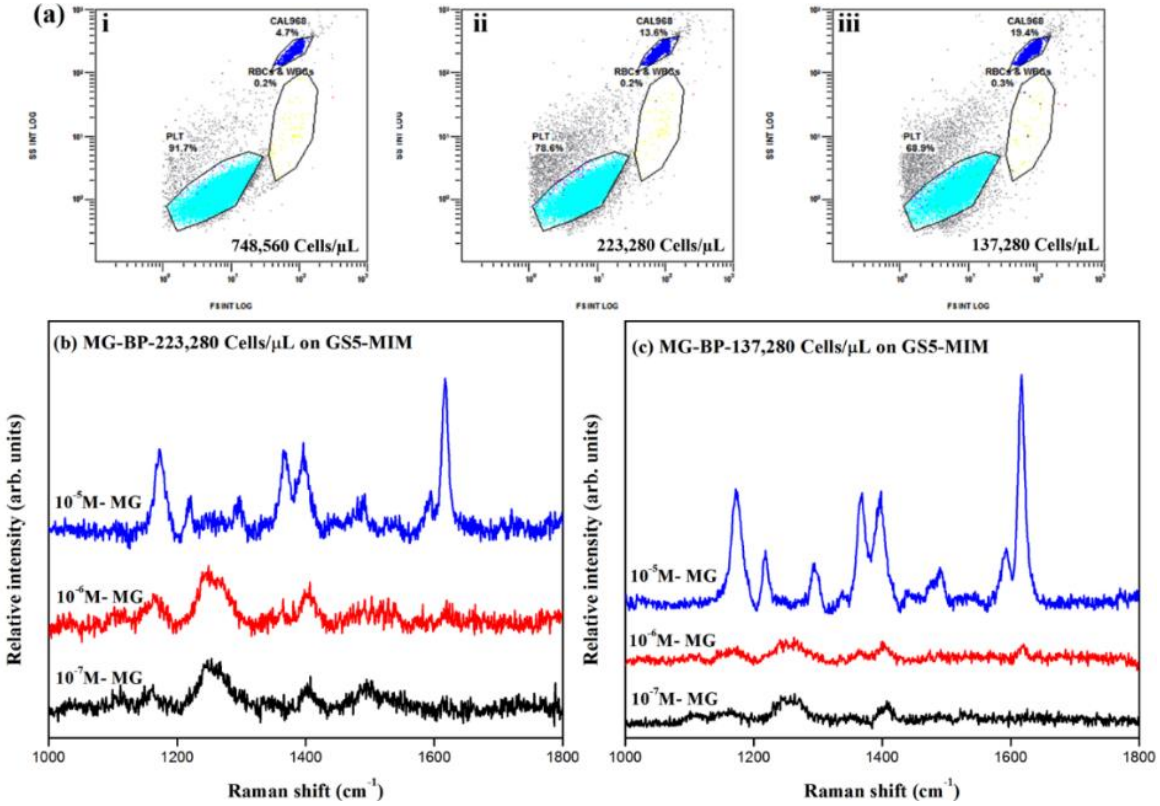

Figure S17 (a) Concentration of PRP solution measured using bioflow method. (b, c) Raman-active peaks of MG molecules at various concentrations in PRP solution at various concentrations on GS5-MIM substrate examined at Raman laser wavelength of 633 nm.

Various concentrations of PRP ((i) 748,560, (ii) 223,280, and (iii) 137,280 cells/μL) were obtained via the bioflow method, as shown in **Figure S17**. In this work, we applied a higher concentration of PPR for Raman analysis. Further work is necessary on low-concentration target molecule (i.e., different MG concentrations) detection in various stock solutions of PPR using GS5-MIM substrates, as shown in **Figure S17**. The Raman characteristic peaks of MG at 1618 cm^{-1} exhibited different enhancements for different concentrations. GS5-MIM exhibited the highest SERS effect at low concentration of MG in PRP solution at various concentrations. Poly(GMA-*co*-SBMA) connected adjacent NCs, lowering the detection limit. The SERS process is stimulated by electromagnetic and chemical effects, which are induced by the sharp corners of NCs, nano gaps between NCs, and metal surface and copolymer dipole-dipole interactions with the target molecule.

Table S4 Raman assignment of MG on copolymer-grafted MIM substrate

Raman shift (cm^{-1})	**Assignment**
1615	Ring C-C stretching
1487	Ring C-C stretching
1448	Ring C-C stretching
1366	N-phenyl stretching
1292	Ring C-C stretching
1215	Ring C-C stretching
1175	Ring C-H bending
989	Ring skeletal vibration
937	Ring skeletal vibration
913	Ring skeletal vibration
802	C-H out-of-plane ring bending vibrations

7. Removal of MG from copolymer-grafted MIM substrate

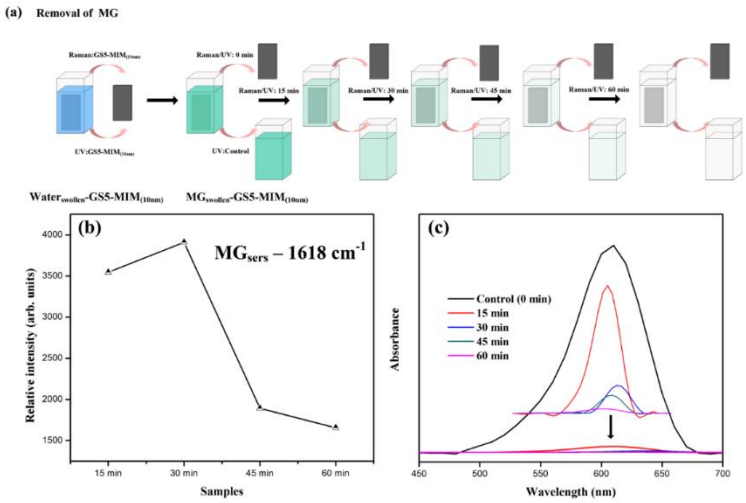

Figure S18 (a) Schematic illustrations of experimental MG removal from GS5-MIM substrate under time-dependent hydration process. (b) Time-dependent hydrated MG peak at 1618 cm^{-1} was used as index for relative Raman intensities with respect to hydration time. (c) UV-Vis characterization of time-dependent MG solution removal from GS5-MIM substrate surface.

We applied a simple hydration method for restructuring the poly(GMA-*co*-SBMA)-grafted surface. The as-fabricated GS5-MIM$_{(10nm)}$ substrate showed SPR bands at 350 and 450 nm, respectively. The plasmonic resonance was reduced due to the geometry of the bottom Ag layer compared to that of the GS5-MIM substrate. The MG molecules absorbed on the GS5-MIM$_{(10nm)}$ substrate surface had a strong SPR intensity and then dramatically decreased SPR intesity with respect to the hydration time, as shown in **Figure 19(a)**. The details of the desorption calculation are shown in **Figure 19(b)**. The MG-adsorbed GS-MIM substrate immersed in water solution was examined using UV-Vis absorbance. The MG desorption (%) was calculated using:

$$Desorption\ (\%) = \frac{\text{Concentration of dye desorbed (mM)}}{\text{Concentration of dye adsorbed (mM)}}\ X\ 100 \qquad (1)$$

The removal efficiency (%R) of MG in aqueous solution was calculated using:

$$R(\%) = \frac{Co - Ce}{Co} \; x \; 100 \qquad (2)$$

where C_0 and C_e are the concentration of the initial MG solution and that after treatment for a certain period time, respectively.

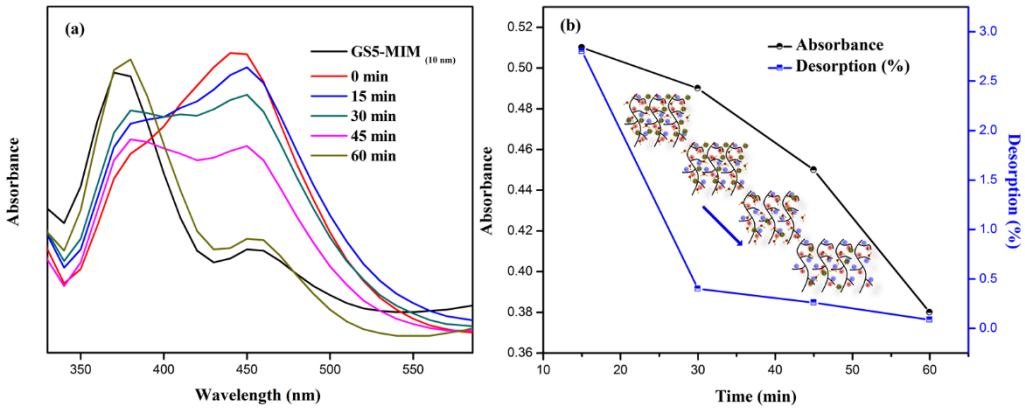

Figure S19 (a) UV absorbance spectrum of time-dependent hydration-processed poly(GMA-*co*-SBMA)-grafted surface. (b) Comparison of adsorbance and desorption (%) from poly(GMA-*co*-SBMA)-grafted surface under hydration process. Illustrations of possible removal process of adsorbed MG molecules from poly(GMA-*co*-SBMA)-grafted MIM sample via hydration process (4 cycles with time interval of 15 min).

References

1. Zhang, Q.; Li, W.; Wen, L.-P.; Chen, J.; Xia, Y., Facile Synthesis of Ag Nanocubes of 30 to 70 nm in Edge Length with CF3COOAg as a Precursor. *Chemistry – A European Journal* **2010,** *16* (33), 10234-10239.
2. Chou, Y.-N.; Wen, T.-C.; Chang, Y., Zwitterionic surface grafting of epoxylated sulfobetaine copolymers for the development of stealth biomaterial interfaces. *Acta Biomaterialia* **2016,** *40*, 78-91.
3. Chou, Y.-N.; Chang, Y.; Wen, T.-C., Applying Thermosettable Zwitterionic Copolymers as General Fouling-Resistant and Thermal-Tolerant Biomaterial Interfaces. *ACS Applied Materials & Interfaces* **2015,** *7* (19), 10096-10107.
4. Zhang, Q.; Li, W.; Moran, C.; Zeng, J.; Chen, J.; Wen, L.-P.; Xia, Y., Seed-Mediated Synthesis of Ag Nanocubes with Controllable Edge Lengths in the Range of 30−200 nm and Comparison of Their Optical Properties. *Journal of the American Chemical Society* **2010,** *132* (32), 11372-11378.
5. Cheng, S.-C.; Wen, T.-C., Robust SERS substrates with massive nanogaps derived from silver nanocubes self-assembled on massed silver mirror via 1,2-ethanedithiol monolayer as linkage and ultra-thin spacer. *Materials Chemistry and Physics* **2014,** *143* (3), 1331-1337.
6. Cheng, S.-C.; Wen, T.-C.; Lan, Y.-C., Plasmonic cavities derived from silver nanoparticles atop a massed silver surface for surface enhancement Raman scattering. *RSC Advances* **2014,** *4* (84), 44457-44461.
7. Lassiter, J. B.; McGuire, F.; Mock, J. J.; Ciracì, C.; Hill, R. T.; Wiley, B. J.; Chilkoti, A.; Smith, D. R., Plasmonic Waveguide Modes of Film-Coupled Metallic Nanocubes. *Nano Letters* **2013,** *13* (12), 5866-5872.